JOURNAL
OF THE AMERICAN CHEMICAL SOCIETY

VOLUME 101, NUMBER 17 AUGUST 15, 1979

Phthalocyanine Thin Films as Semiconductor Electrodes

Fu-Ren Fan and Larry R. Faulkner*

Contribution from the Department of Chemistry, University of Illinois, Urbana, Illinois 61801. *Received December 22, 1978*

Abstract: Metal-free, zinc, and nickel phthalocyanines (H_2Pc, ZnPc, and NiPc) have been studied electrochemically. The electrode assemblies involved a glass substrate overlaid by a gold contact layer, which in turn was covered by the phthalocyanine at nominal thicknesses of 40–3000 Å. Interfacial capacitances were determined as functions of potential and frequency. Plots of capacitance vs. potential showed sharp rises for potentials more positive than 0.3 V vs. SCE and (for H_2Pc and ZnPc) peaks at more negative potentials. The capacities were linear with the inverse square root of frequency in the negative potential regime. Cyclic voltammetric studies of six nonlabile complexes of Fe(II) were carried out, and chronocoulometry was used to measure their standard heterogeneous rate constants. The complexes with very negative standard potentials could be oxidized irreversibly on H_2Pc but could not be reduced again. Systems with more positive standard potentials were reversibly oxidized and reduced. The irreversible systems could be reduced on H_2Pc at potentials more negative than 0.35 V vs. SCE when the electrode was irradiated by light at 6328 Å. The observations have been rationalized by considering the phthalocyanines as relatively well behaved p-type semiconductor electrodes. Band edges and interfacial states have been mapped and the nature of interfacial charge transfer has been discussed in terms of Gerischer's model modified by inclusion of surface states in the gap region.

The phthalocyanines have received attention recently because several are electrocatalysts for the reduction of molecular oxygen.[1-9] The mechanism of catalysis and the means for optimizing it are of primary interest.

A related concern is the ability of solid phthalocyanine phases to engage as actual electrodes in electrochemical processes. Several recent studies have borne on this point,[3-5,7-10] and there is strong evidence that these materials are capable of even reversible charge transfer. The degree to which electrochemical kinetics are influenced by the solid-state physics of conduction in the phthalocyanine phases is largely unknown; however, there are a few pertinent experiments. Meier et al. have shown that electrocatalytic activity of polymeric phthalocyanines correlates with conductivity,[8] and earlier work from this laboratory showed that electrochemical performance of phthalocyanine electrodes was strongly influenced by ambient factors controlling conduction.[7] Alferov and Sevast'yanov[9] and Meshitsuka and Tamaru[10] have reported photoelectrochemistry that seems to be based on semiconduction in these materials. Possibly related are our earlier observations that the reduction of oxygen is actually inhibited, rather than being catalyzed, at thin-film electrodes of zinc and iron phthalocyanines (ZnPc and FePc).[7] We suggested that the inhibitions might be understood by regarding the phthalocyanine films as p-type semiconductor electrodes with flat-band conditions near 0.0 V vs. SCE.

The semiconducting properties of such films were anticipated from reports already in the literature.[11-18] More recently, the properties of ZnPc and metal-free phthalocyanine (H_2Pc) have been illuminated in detail via studies of rectifying properties and photovoltaic effects at phthalocyanine/metal junctions.[19] These materials are indeed p-type semiconductors with a high density of intermediate energy levels. The electrochemical properties of ZnPc and H_2Pc electrodes in solutions containing different redox couples are therefore predictable,[20-24] provided that the electrode processes are not complicated by additional reactions such as chemisorption.

Our aim in the present study was to correlate the electrochemical reactivities of several solution species with the relative positions of their energy levels and the known band edges and intermediate levels of phthalocyanine thin-film electrodes. Metal-free, zinc, and nickel phthalocyanines in evaporated thin films have been used as electrodes, and measurements have been carried out by cyclic voltammetry, chronocoulometry, and impedance techniques. A very wide range of behavior has been observed, but virtually all of the results can be understood within the semiconductor model.

Experimental Section

Tris(3,4,7,8-tetramethyl-1,10-phenanthroline)iron(II) sulfate ($Fe(TMP)_3SO_4$) was obtained from the G. F. Smith Chemical Co. and was recrystallized from distilled water. Tris(4,7-dimethyl-1,10-phenanthroline)iron(II), tris(1,10-phenanthroline)iron(II), tris(2,2'-bipyridine)iron(II), and $Fe^{II}EDTA$ were allowed to form directly in electrochemical test solutions by mixing stoichiometric amounts of the ligands and ferrous sulfate. G. F. Smith Chemical Co. supplied the 1,10-phenanthroline (o-ph), 4,7-dimethyl-1,10-phenanthroline (DMP), and 2,2'-bipyridine (bpy), which were used without further purification. Disodium EDTA was obtained from Hach Chemical Co. and was recrystallized from water. Potassium ferri- and ferrocyanides (reagent grade) were recrystallized twice from distilled water. The phthalocyanines were purchased from Eastman Kodak and were used without further treatment.

Phthalocyanine thin film electrodes were prepared by evaporation according to the techniques reported earlier.[7,19] A chromium anchor layer (30–40 Å) was first deposited through a mask onto a clean glass substrate, then gold at a 400 Å thickness was directly overlaid in the

0002-7863/79/1501-4779$01.00/0

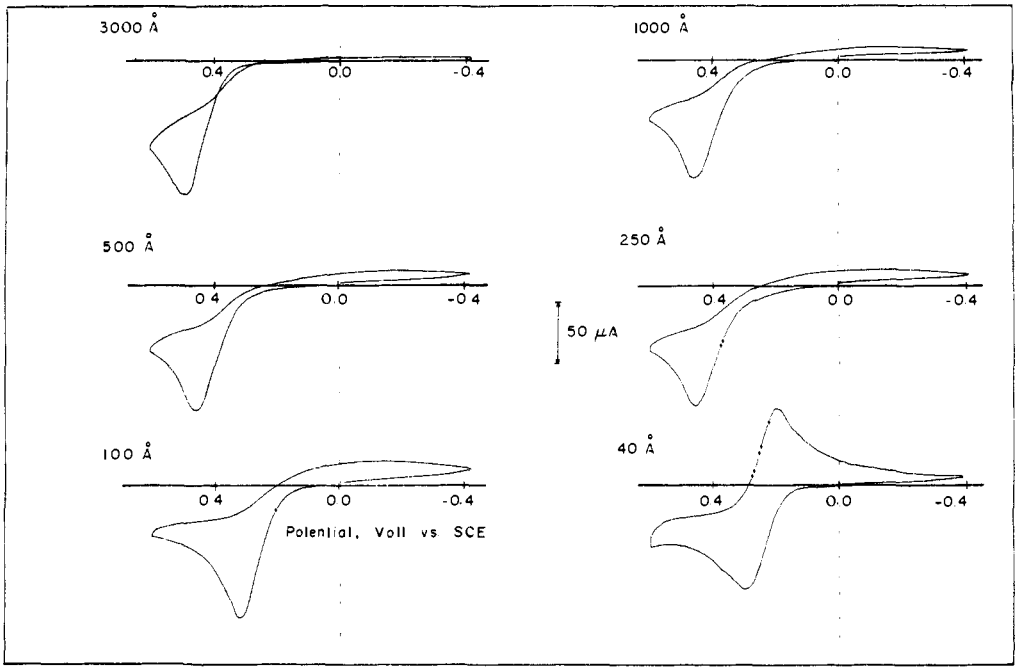

Figure 1. The dependence of the cyclic voltammogram for 3.00 mM ferrocyanide on H_2Pc film thickness. All scans start at −0.4 V vs. SCE and sweep at 100 mV/s. Medium is 1.0 M KNO_3.

same pattern. Finally, the phthalocyanine was deposited (in α form)[7,19] over the whole assembly.[25] The portion of the phthalocyanine serving as the electrode proper in electrochemical studies was that which directly overlay a gold disk of 0.20 cm^2. The assemblies were stored in vacuo ($\lesssim 10^{-6}$ Torr) until they were to be used.

The phthalocyanine electrodes were inserted into the solution only deeply enough to allow immersion of the gold disk. This procedure enabled us to reproduce the effective electrode area to ~±10%. A coiled Pt wire was used as an auxiliary electrode, and a saturated calomel electrode served as a reference. The solution was deaerated by purging with nitrogen, and it was kept under nitrogen during every measurement. The pH values of the solutions were kept at 6.0 ± 0.2 by adjusting with 1 N KOH or H_2SO_4, if necessary. If not otherwise mentioned, the experiments were performed in the dark.

Cyclic voltammetric measurements were made with a Princeton Applied Research Model 173 potentiostat and custom-built waveform generator or with a custom-built electrochemical system. Computer-based apparatus like that described earlier was employed for chronocoulometry.[7] No compensation of resistance was attempted.

All impedance measurements were carried out with 1 M KNO_3 electrolyte. The electrical circuit allowed the application of a variable potential at the phthalocyanine electrode with respect to the reference electrode. The impedance was measured between this working electrode and a large (~10 cm^2) counter electrode. The applied potential was controlled potentiostatically, and the impedance was measured by a General Radio Model 1650A bridge with excitation by an external ac generator. The apparatus was checked by a dummy cell having a configuration similar to that of the real cell. The quantities measured were the equivalent series capacitance, C_s, and the dissipation factor $\omega R_s C_s$, where ω is the angular frequency and R_s is the equivalent series resistance. For most systems, the dissipation factors were much less than unity, but factors on the order of unity were recorded for systems involving thick phthalocyanine films and low excitation frequencies. Impedance measurements were not changed by lifting the counter electrode partially out of the electrolyte; thus the counter electrode did not make significant contributions to the capacitances reported below.

Results

Cyclic Voltammetry. In deaerated 1.0 M KNO_3, cyclic voltammograms at H_2Pc electrodes show a flat background response from +0.8 to −1.0 V vs. SCE. ZnPc and NiPc have similar working ranges.

Figure 1 shows voltammograms of the ferri-/ferrocyanide couple in 1 M KNO_3 at H_2Pc electrodes having different thicknesses. In general, oxidation occurs readily, but reduction is very slow and cannot be activated by any overpotential in the studied range. The shapes of the voltammograms are essentially unchanged until the H_2Pc films become so thin (<100 Å nominal) that electron exchange between the metal and the electrolyte can take place directly, either in regions exposed via partial coverage or by electron tunnelling. The anodic peak currents are essentially independent of film thickness; however, the corresponding peak potentials are thickness dependent when the H_2Pc film is thicker than 500 Å. This effect probably reflects both the sluggish nature of electron transfer at H_2Pc for this couple and the internal resistance of the H_2Pc film.

For the more negative redox couples, ferri-/ferrocyanide and $Fe^{III}EDTA/Fe^{II}EDTA$, the anodic peak potentials are dependent on the interval between sweeps. If the waiting period does not exceed 3–5 min, the anodic peak lies reproducibly at its negative limit. For longer intervals, the oxidation peak is reduced in size and displays a larger overpotential. As shown in Figure 2, successive sweeps at a fresh electrode produce a negative shift in the anodic peak potential and a growth in the current. These phenomena are rarely seen for redox systems with standard potentials more positive than that of ferri-/ferrocyanide. Over a range of scan rates from v = 3 to 100 mV/s, the steady-state anodic peak current varies as $v^{1/2}$.

Figure 3 depicts cyclic voltammograms for six iron complexes which have nonlabile ligands coordinated to the central ion. These compounds show reversible or quasi-reversible cyclic voltammograms at a Pt disk. Their standard potentials span a fairly large range; hence they could be useful in mapping bands and levels of phthalocyanine electrodes. Moreover, they probably follow similar electron-transfer mechanisms because they have similar inner-sphere coordination structures. The peak potentials for the oxidation and rereduction of the six compounds are summarized in Table I. The potentials for the more negative couples have an uncertainty of ~50 mV.

A close examination of Figure 3 reveals that there is apparently a systematic variation in the kinetics of electron transfer at H_2Pc as $E^{0\prime}$ becomes more positive. For couples with $E^{0\prime}$ more negative than 0.25 V, the redox reactions are essentially totally irreversible. The oxidation peaks show large

Table I. Peak Potentials for Oxidations and Rereductions of Compounds Used in This Study[a]

compd	Pt electrode		H_2Pc electrode			
	$E^{0\prime}$[b]	$E_{p,a}$[c]	$E_{p,a}$[c]	$E_{p,c}$[d]	ΔE_p[e]	$\Delta E_{p,a}$[f]
$Fe(EDTA)^{2-}$	−0.130	−0.080	0.37	none		0.45
$Fe(CN)_6^{4-}$	0.225	0.250	0.45	−0.12[g]	0.57	0.20
$Fe(TMP)_3^{2+}$	0.610	0.650	0.740	0.570	0.170	0.090
$Fe(DMP)_3^{2+}$	0.657	0.700	0.790	0.625	0.165	0.090
$Fe(bpy)_3^{2+}$	0.785	0.820	0.840	0.765	0.075	0.020
$Fe(o\text{-}ph)_3^{2+}$	0.820	0.855	0.860	0.790	0.070	0.005

[a] Potentials vs. SCE in volts. Scan rate = 100 mV/s. [b] Average of anodic and the cathodic peak potentials on Pt electrodes. [c] Anodic peak potential. [d] Cathodic peak potential. [e] Difference between the anodic and the cathodic peak potentials on H_2Pc electrodes. [f] Difference between anodic peak potentials on Pt and H_2Pc electrodes. [g] Broad.

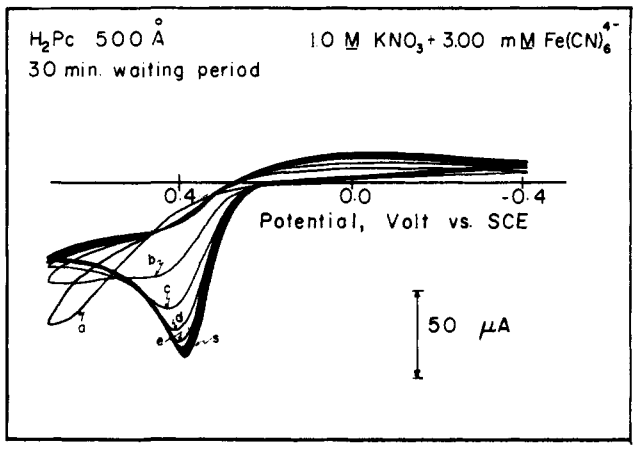

Figure 2. Continuously recorded cyclic voltammograms on H_2Pc at 500 Å thickness. Scan rate = 100 mV/s. (a) shows initial cycle; (b)-(e) show subsequent cycles; (s) shows steady state.

overpotentials, and reduction hardly occurs at all. Couples with $E^{0\prime}$ between 0.25 and 0.65 V undergo quasi-reversible transfer. This region appears to be a transition zone between domains of irreversible and reversible behavior. Compounds oxidized at more positive potentials than 0.65 V show comparable, virtually reversible responses at both H_2Pc and Pt.

At ZnPc and NiPc electrodes, cyclic voltammograms of the ferri-/ferrocyanide couple in 1 M KNO_3 show irreversible responses in the first several cycles, but the behavior becomes more reversible as the measurement is repeated. After three to ten cycles, one reaches a quasi-reversible steady state. Well-formed peaks are seen for both oxidation and reduction, in contrast to the behavior at H_2Pc. The anodic peak currents are proportional to $v^{1/2}$.

For the EDTA complex, unusual steady-state responses were obtained at ZnPc and NiPc (Figure 4). Besides the peaks corresponding to those at Pt (where the standard potential is −0.130 V vs. SCE), there is a second anodic peak in each case.

Chronocoulometry. Figure 5 displays chronocoulometric curves for blank electrolyte and for five of the complexes. The initial potential in each case was 0.0 V vs. SCE, and the step width was 250 ms. The step potential was 0.35 V for the pictured data involving plain supporting electrolyte, but when electroactive species were added steps were made to the voltammetric half-peak potential observed on H_2Pc at v = 100 mV/s.

In blank electrolyte, nearly reversible charge injection is seen, and the result can be attributed almost entirely to capacitive charging. The time constant is on the order of 20 ms.

The results obtained for the complexes offer parallels to the cyclic voltammograms of Figure 3. For $Fe^{II}EDTA$, there is a linear forward segment, indicating charge injection by a process limited to a constant rate, and a flat reverse segment indicating virtually no faradaic activity. For other complexes, the extent of diffusion control increases systematically as the standard potential becomes more positive. For $Fe^{II}(o\text{-}ph)_3$, the reverse step is almost entirely diffusion limited.

Table II. Heterogeneous Rate Constants and Anodic Transfer Coefficients at H_2Pc Thin Film Electrodes

redox system	$k_{s,h}$, cm s^{-1}	β
$Fe(EDTA)^{2-/-}$	1.26×10^{-4}	0.15
$Fe(CN)_6^{4-/3-}$	2.28×10^{-4}	0.47
$Fe(TMP)_3^{2+/3+}$	4.17×10^{-4}	0.49
$Fe(DMP)_3^{2+/3+}$	7.14×10^{-4}	0.49
$Fe(bpy)_3^{2+/3+}$	2.15×10^{-3}	0.59
$Fe(o\text{-}ph)_3^{2+/3+}$	2.62×10^{-3}	0.50

This behavior suggests that the intrinsic rate constants for heterogeneous charge transfer, $k_{s,h}$, rise systematically as the standard potential moves more positive. The rate constants were actually evaluated in another set of chronocoulometric experiments. For a given couple, steps were made to various potentials on the foot of the voltammetric peak, so that the rate of charge injection was always constant and was limited by the charge-transfer process. The slope of the resulting linear chronocoulometric segment was the constant faradaic current for the step potential. Each system showed Tafel-like behavior at potentials sufficiently negative with respect to the peak.[26] By extrapolating a linear segment of log i vs. E to the standard potential, one obtains a current $i_s = nFAk_{s,h}C^*$ where C^* is the bulk concentration of the reduced complex and the other symbols have the usual significance.[26] Table II shows the rate constants obtained in this way. Also shown are anodic transfer coefficients β, which were obtained from the slopes of the plots, $\beta nF/2.303RT$.[26] In general, the data in Table II bear out the conclusion that there is a systematic linkage between kinetic facility and the standard potential.

Impedance Measurements. Films of H_2Pc, ZnPc, and NiPc were subjected to impedance measurements in indifferent electrolyte solutions under bias potentials where the residual currents were negligibly small. Thus the measured value of C_s is the equivalent differential capacitance of the interface, without a faradaic contribution, and R_s, as reflected in the dissipation factor, is an ohmic resistance.

As shown in Figure 6, the capacitance at H_2Pc electrodes shows a broad maximum at 0.00 V. The position of the maximum is independent of frequency. In the potential range more negative than 0.30 V the capacitance is fairly strongly frequency dependent, but at more positive potentials it is less dispersed.

The frequency dispersion of the capacitance at selected potentials is shown shown in Figure 7. It can generally be represented by the equation

$$C_s = A + B/f^m \qquad (1)$$

where A and B are two constants independent of the measuring

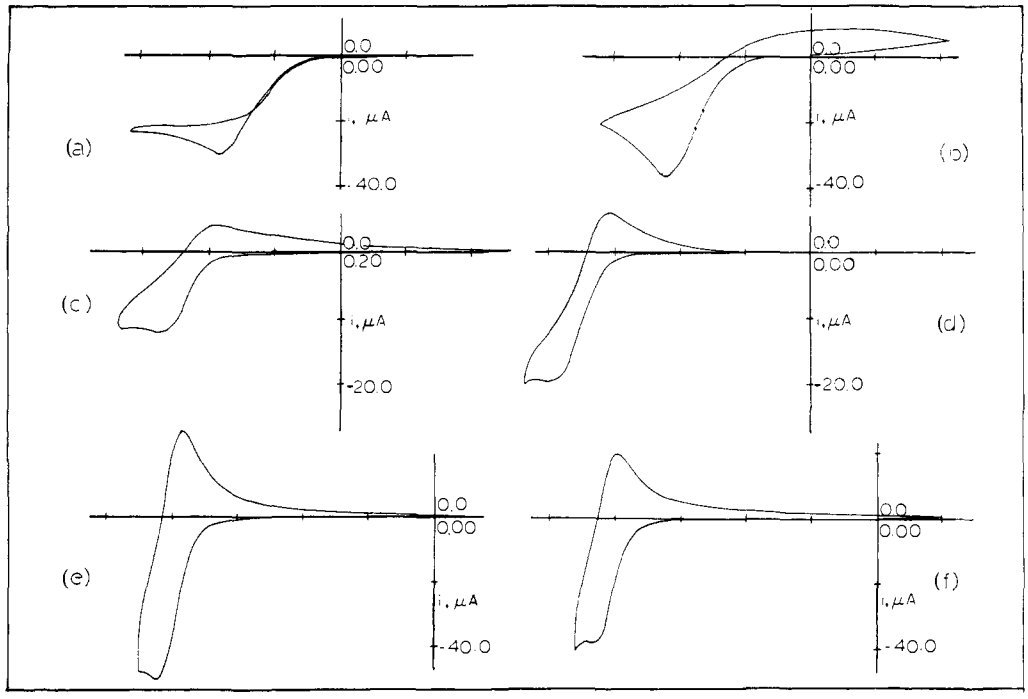

Figure 3. Cyclic voltammograms of six iron(II) complexes on a 500 Å thick H_2Pc electrode. All scans start at the negative potential limit and sweep at 100 mV/s. Potentials are vs. SCE, and a unit on the potential axis is 0.2 V. (a) 1.00 mM $Fe^{II}EDTA$, (b) 1.00 mM $Fe(CN)_6^{4-}$, (c) 0.45 mM $Fe(TMP)_3^{2+}$, (d) 0.55 mM $Fe(DMP)_3^{2+}$, (e) 1.00 mM $Fe(bpy)_3^{2+}$, (f) 1.00 mM $Fe(o\text{-}ph)_3^{2+}$. Medium is 1 M KNO_3 for (a), (b), (c), and (f) and 0.5 M K_2SO_4 for (c) and (d).

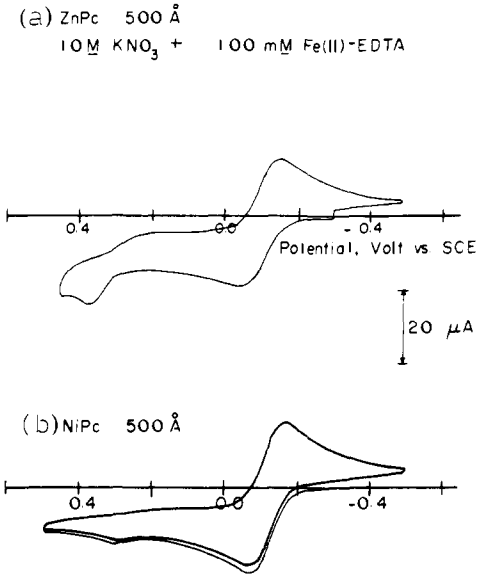

Figure 4. Cyclic voltammograms for $Fe^{II}EDTA$ at ZnPc and NiPc electrodes. Scan in (a) starts at −0.3 V vs. SCE. Scan in (b) starts at −0.4 V vs. SCE. Sweep rate = 100 mV/s.

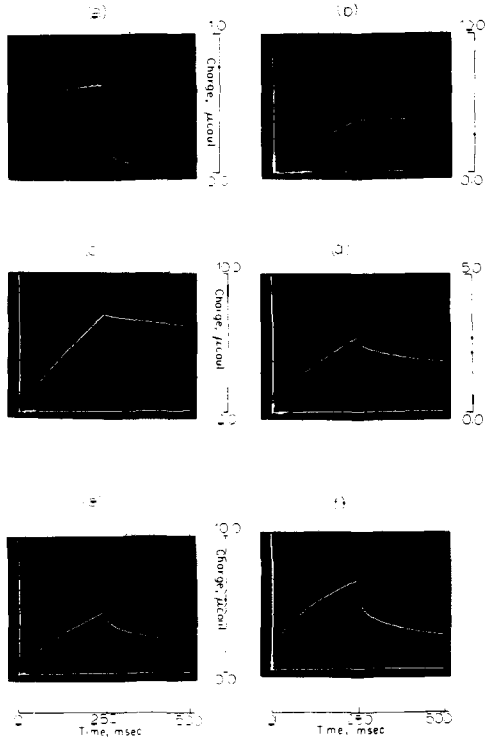

Figure 5. Chronocoulometric curves at a 500 Å thick H_2Pc electrode: (a) 1.0 M KNO_3, 0.0–0.35 V vs. SCE; (b) 1.0 M KNO_3 plus 1.00 mM Fe^{II}-EDTA, 0.0–0.260 V; (c) 1.0 M KNO_3 plus 1.00 mM $Fe(CN)_6^{4-}$, 0.0–0.340 V; (d) 0.5 M K_2SO_4 plus 0.45 mM $Fe(TMP)_3^{2+}$, 0.0–0.660 V; (e) 0.5 M K_2SO_4 plus 0.55 mM $Fe(DMP)_3^{2+}$, 0.0–0.695 V; (f) 1.0 M KNO_3 plus 1.00 mM $Fe(o\text{-}ph)_3^{2+}$, 0.0–0.795 V.

frequency f, and the exponent m lies between 0 and $1/2$. For H_2Pc electrodes in 1 M KNO_3, $m = 1/2$ at potentials more negative than 0.3 V, but $m = 1/4$ at more positive potentials. The capacitance-frequency plots converge to small values when the electrode potential is more negative than 0.3 V; thus the A value in eq 1 is nearly independent of potential in this range.

For ZnPc, as shown in Figure 8, the capacitance shows two maxima at −0.20 and −0.60 V vs. SCE. In the potential range more positive than 0.3 V the capacitance is nearly frequency independent, and at potentials more negative than 0.1 V it is inversely proportional to $f^{1/2}$, for $f < 4$ kHz.

The capacitance-potential characteristics of NiPc electrodes are shown in Figure 9. There are no maxima, and the frequency dispersion seems much smaller than for ZnPc and H_2Pc.

Photoelectrochemistry. Figure 10 shows that a cathodic

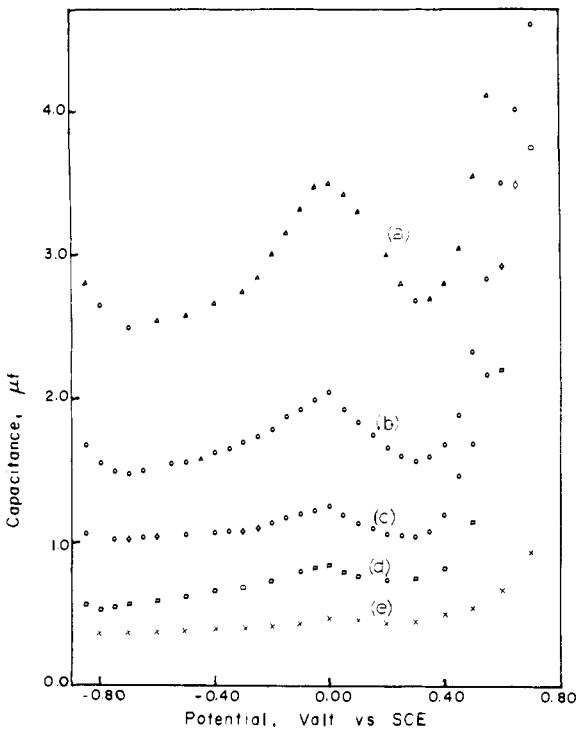

Figure 6. Differential capacitance at a 500 Å thick H_2Pc electrode in 1 M KNO_3 at different excitation frequencies: (a) 100 Hz, (b) 350 Hz, (c) 1 kHz, (d) 3.5 kHz, (e) 10 kHz.

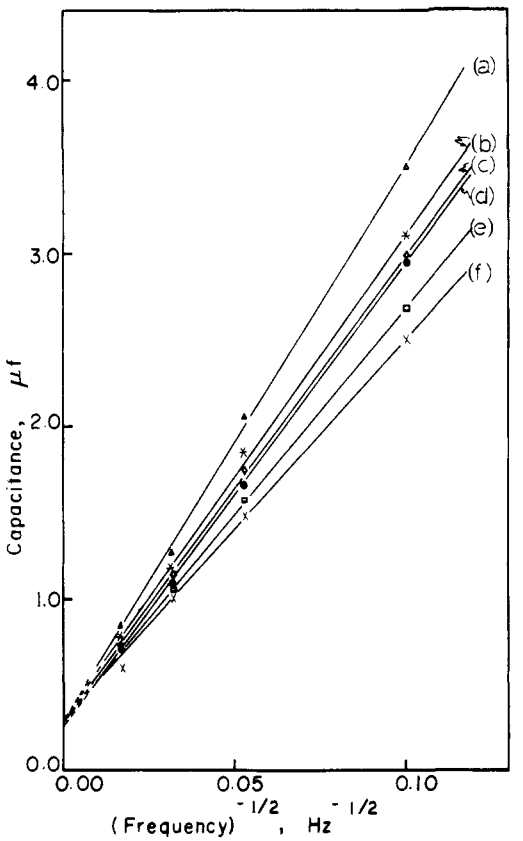

Figure 7. The frequency dispersion of differential capacitance at a 500 Å thick H_2Pc electrode: (a) 0.00 V vs. SCE; (b) −0.90 V, (c) −0.20 V, (d) 0.20 V, (e) 0.30 V, (f) −0.70 V.

current corresponding to the reduction of ferricyanide was observed when an H_2Pc/solution interface was illuminated by a He-Ne laser (6328 Å, ~60 mW/cm^2). Background voltammograms recorded in the absence of ferricyanide showed a very small photoeffect; hence the light-induced current can be ascribed to the reduction of ferricyanide. The anodic current corresponding to the reoxidation of ferrocyanide is also photosensitive. This effect is probably a direct result of photoenhancement in the cathodic process that produces the ferrocyanide immediately beforehand, since the anodic peak in the presence of ferrocyanide is not photosensitive if the initial scan is positive. Significant light-induced cathodic current was observed only at potentials more negative than 0.35 V vs. SCE.

Discussion

Results presented here give considerable support to the idea that phthalocyanine surfaces are capable of faradaic activity. At H_2Pc the facility of charge transfer seems wholly determined by the phthalocyanine at coverages greater than ~100 Å. Only at lower coverages is the metal contact directly involved. The dimensions of the phthalocyanine layer seem to have little effect on the electrochemistry at thicknesses $\gtrsim$100 Å.

With H_2Pc electrodes, the salient observations bearing on the mechanism of charge transfer include (1) a systematic variation in $k_{s,h}$ with $E^{0\prime}$, (2) an onset in photoelectrochemical activity at potentials more negative than ~0.3 V vs. SCE, (3) the structure in plots of interfacial capacitance vs. potential, (4) the sharp rise in interfacial capacitance at potentials more positive than 0.3 V vs. SCE, (5) the frequency dependence of the capacitance, and (6) the fact that the capacitance levels off at high and low frequencies. Less extensive, but similar, results were obtained for ZnPc and NiPc.

We can successfully interpret all of the data by regarding the phthalocyanines as relatively well-behaved p-type semiconductor electrodes. The onset of photoelectrochemical activity and the sharp rise in interfacial capacitance at 0.3 V vs.

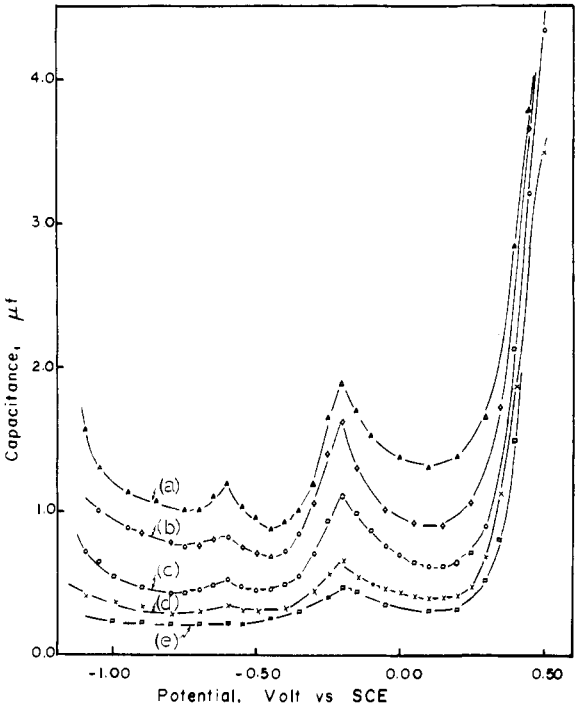

Figure 8. Differential capacitance at a 500 Å thick ZnPc electrode in 1 M KNO_3 at different excitation frequencies. (a)-(e) correspond to frequencies listed in caption to Figure 6.

SCE point to a flatband condition near that potential for H_2Pc. The structure in the plots in capacitance vs. the potential at more negative values suggests a distribution in interfacial states which can assist in the charge-transfer reactions. The fre-

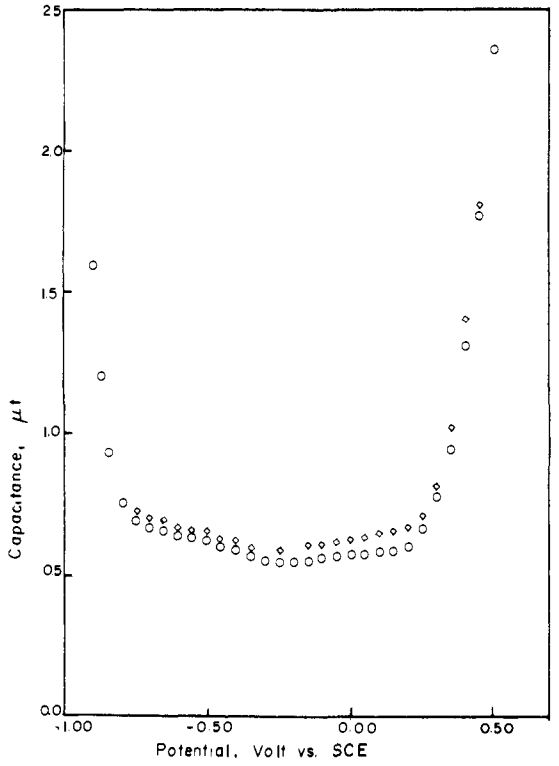

Figure 9. Differential capacitance at a 500 Å thick NiPc electrode in 1.0 M KNO_3 at different frequencies: Diamonds, 350 Hz; circles, 1 kHz.

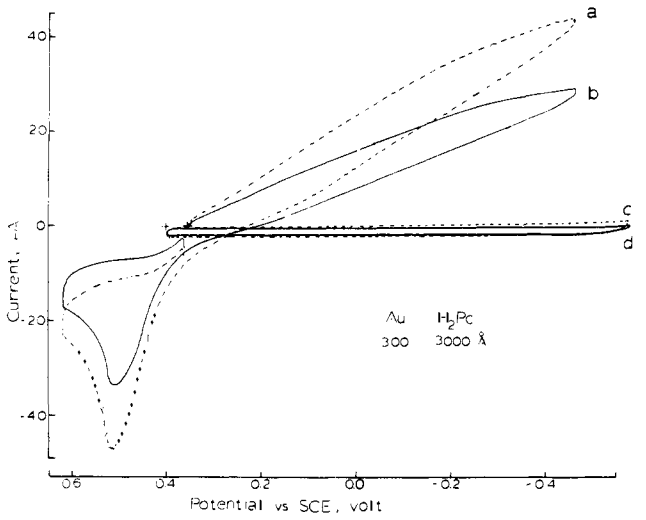

Figure 10. Photoelectrochemical effect at an H_2Pc electrode. Irradiation at 6328 Å. Solid curves recorded in the dark, dashed curves recorded under illumination. (a) and (b): 1.0 M KNO_3 plus 10 mM $K_3Fe(CN)_6$. (c) and (d): 1.0 M KNO_3. Scan starts at 0.4 V vs. SCE with sweep rate = 100 mV/s.

quency dependence of the capacitance and its tendency to level off at extreme frequencies seem to be related to the transport and relaxation of carriers within the solid. The change in the frequency dependence of the capacitance at 0.3 V vs. SCE tends to confirm the assignment of the flatband condition. With the bands and surface states located along these lines, one can understand the systematic linkage between $k_{s,h}$ and $E^{0\prime}$ as reflecting both improved carrier densities at more positive potentials and better overlap of solid-state energy levels with corresponding levels of the redox species in solution. The paragraphs below amplify various aspects of this general interpretation and provide detailed support for its validity.

Frequency Dispersion for Capacitance. Linear dispersion plots like those of Figure 7 could be rationalized by invoking either residual faradaic processes[27-30] or manifestations of carrier relaxation and transport processes in semiconductor electrodes.[22,31] Residual faradaic processes were used by Randin to interpret the frequency dispersion of capacitance at semiconductor electrodes in qualitative terms.[30] However, his experiments were performed in 1 N H_2SO_4, in which proton discharge can occur over the studied potential range. Moreover, his capacitances per unit area were 100 times higher than ours. If the currents measured in our determinations of differential capacitance are indeed faradaic, they would have to be controlled by the diffusion of dissolved species over most of the working range in order to rationalize the observed linearity with $f^{-1/2}$. It seems unlikely that an impurity in the solutions could be sufficiently concentrated to explain the capacitance levels observed. In addition, one would be pressed to understand the different shapes of the plots of capacitance vs. potential for H_2Pc, ZnPc, and NiPc in terms of a common dissolved impurity. Thus the distribution and the dispersion of capacitance apparently relate to the electrode itself. The dispersion can be successfully interpreted in terms of a semiconductor model, provided that the transport and relaxation properties of minority carriers are taken into account.

Application of a sinusoidal voltage across the space-charge region of a semiconductor electrode leads to a periodic redistribution of charge, which manifests itself as a capacitance. Majority carriers in the bulk are moved by the electric field in the bulk, but minority carriers move by diffusion if their lifetime is sufficiently short that the potential drop over a diffusion length is less than kT/e. The diffusion of minority carriers into and out of the space-charge region can control the quantity of charge collected and discharged during a cycle; hence it can control the capacitance. It can also cause a dispersion in capacitance via the linkage between diffusion length and the time available for diffusion.[21,31]

When the sinusoidal frequency is low, collection of minority carriers can be made over the maximum possible diffusion distance $l_0 \propto (D\tau)^{1/2}$, where D is the diffusion coefficient and τ is the minority carrier lifetime. At frequencies such that $1/f \ll \tau$, the diffusion distance becomes shortened because there is less time for collection and discharge of carriers. In this time domain, the diffusion distance is controlled by the frequency, $l \propto (D/f)^{1/2}$; hence the diffusion capacitance becomes proportional to $f^{-1/2}$. At very high frequencies, the diffusion capacitance becomes negligibly small. Then one is left with a frequency-independent component of the space-charge capacitance.[21,31]

The diffusion capacitance can only be effective in the potential range where an inversion layer is enforced at the electrochemical interface.[21] If a depletion layer or an accumulation layer is found there, diffusion of minority carriers is a negligible consideration, because there is no longer any region of space where minority carriers dominate the electrical properties of the system.

The phthalocyanine electrodes show behavior that is grossly concordant with this pattern, as one would formulate it for a p-type electrode with a flatband condition near 0.3 V vs. SCE. In the more negative potential region, where an inversion layer could be expected, the capacitance is linear with $f^{-1/2}$, but in the positive region it is much less dispersed.

On the other hand, there are two details of our observations which do not fit neatly into this picture: (a) The linearity with $f^{-1/2}$ is maintained to very low frequencies, and (b) the linearity also holds to rather positive potentials. Point (a) implies that the minority carrier lifetime exceeds 10 ms, a figure which is extraordinarily long.[18] Point (b) suggests that either the flatband condition is considerably more positive than 0.3 V vs. SCE or the characteristics of the material are such that the transition between inversion and accumulation at the interface

occupies an exceptionally narrow zone on the potential axis, given the band gap (~2 eV) of the solid.

It is possible to understand both discrepancies if the effective minority carriers are not electrons, but are instead mobile acceptor sites. Earlier work has shown that most of the conductivity in these materials is induced by absorbed oxygen and water from the air.[7,12-14] Interaction with the solid yields a fairly mobile hole and a relatively fixed trapped electron. It is possible that acceptor sites either with or without trapped electrons can diffuse slowly through the lattice and contribute to the redistribution of space charge in response to a change in potential. They would have the long lifetimes required by observation (a). Moreover, this mechanism would lead to a narrow "effective band gap" that could rationalize observation (b). We cannot now present direct evidence supporting the idea that the acceptor sites are slightly mobile; however, we have seen some apparent gettering effects with aluminum contacts which could manifest the phenomenon.[19]

Potential Dependence of Capacitance. The most striking aspect of our plots of capacitance vs. potential is the existence of maxima for H_2Pc and ZnPc. These features can be explained in terms of intermediate levels located within the band gap. Such levels act as reservoirs for charge and enhance the differential capacitance whenever their occupancy can be significantly altered by differential changes in the Fermi level.[20-22] This condition applies only when the mean Fermi level is within a few kT of the intermediate level, thus the plots of capacitance vs. potential serve to map zones of intermediate states.

As shown in Figure 6, the capacitance of H_2Pc electrodes shows a broad peak at a potential near 0.0 V vs. SCE; hence we can place a zone of interfacial states at 0.24 V vs. NHE. The density of this band of interfacial states maximizes at an energy of 4.75 eV vs. the vacuum level, since the NHE itself corresponds to 4.51 eV.[32] The valence band edge of H_2Pc is near 5.20 eV on the absolute scale;[33,34] hence the band of interfacial states peaks at 0.45 eV above the valence band edge. It is relevant that our earlier solid-state studies of H_2Pc suggested that conduction in H_2Pc might be limited by a large number of discrete traps approximately 0.5 eV above the valence band.[19]

Similar solid-state studies of ZnPc suggested that there is a wide distribution of traps in the band gap,[19] and the differential capacitance measurements again confirm those earlier indications. Figure 8 shows that ZnPc seems to have two sets of surface states. One of them maximizes its density at −0.20 V and the other peaks at −0.60 V vs. SCE. These values correspond to 4.55 and 4.15 eV vs. the vacuum level. Since the valence band edge of ZnPc is near 5.10 eV,[19] the two sets of intermediate levels lie about 0.6 and 1.0 eV above the valence band edge.

In the case of NiPc, no well-defined bands of interfacial states seem to exist in the band gap. However, the capacitance is probably too high to be attributed entirely to the space charge, and the cyclic voltammetric observations of $Fe^{II}EDTA$ at NiPc electrodes imply the presence of intermediate levels (see below). It is possible that their distribution is simply too broad to appear in Figure 9 as a discrete band.

The maximum interfacial state density can be estimated from the height of the maximum in capacitance[21,22] via

$$C^0_{ss} \approx \left(\frac{e^2}{4kT}\right) N_t \qquad (2)$$

where C^0_{ss} is maximum equilibrium surface state capacitance (corrected for relaxation effects related to frequency) and N_t is the density of the interfacial states. When ZnPc electrodes are strongly depleted or inverted, the capacitances approach limiting values for frequencies below several hundred hertz. The limiting capacitance is about 10 $\mu F/cm^2$ at −0.20 V and 6 $\mu F/cm^2$ at −0.60 V. Taking these values as the equilibrium interfacial state capacitances without correction for diffusion of minority carriers, one can estimate the densities of the corresponding surface states to be $5 \times 10^{12}/cm^2$. For H_2Pc electrodes, the equilibrium interfacial state capacitance is greater than 18 $\mu F/cm^2$ and thus the interfacial state density would exceed $10^{13}/cm^2$.

These interfacial state densities can be compared with the trap densities estimated from solid-state studies. Grain sizes of the vapor-deposited phthalocyanine films are on the order of 200 Å.[32,35] Assuming that the shape of the grain is cubic, the total surface area of the grains contained in 1 cm^3 of Pc film will be about 10^6 cm^2. Assuming that interfacial states are located entirely at grain boundaries, we estimate a bulk trap density in the range of 10^{18}-10^{19} cm^{-3}, which agrees fairly well with the values obtained earlier from the solid-state studies.[14,19]

Plots of C_s vs. $f^{-1/2}$ for ZnPc electrodes level off at a noticeably higher characteristic frequency than equivalent plots for H_2Pc. This behavior suggests that minority carrier exchange between the bulk and the space charge region is much faster in ZnPc than in H_2Pc. Such an interpretation is concordant with the different voltammetric behavior observed at H_2Pc and ZnPc electrodes (see below).

Interfacial Charge Transfer. Considerations of capacitance and photoelectrochemical effects have provided maps of the band edges and interfacial states of the phthalocyanines; hence one should be able to discuss charge transfer in a semiquantitative way by matching the solution states of various redox couples with the available states in the solids. According to Gerischer's model,[20,21] the rate of electron transfer is proportional to the density of carriers at the interface and the probability that the species in solution can offer an accommodation to an electron or hole at an energy equal to its energy in the solid. In the fluctuating energy level scheme, the energy level distribution functions, $W_{ox}(U)$ and $W_{red}(U)$, of the oxidized and reduced species in solution are given by[20,21]

$$W_{ox}(U) \propto \exp[-(U - U^0 - \lambda)^2/4\lambda kT] \qquad (3)$$

$$W_{red}(U) \propto \exp[-(U - U^0 + \lambda)^2/4\lambda kT] \qquad (4)$$

where U is the electron energy, U^0 is the energy corresponding to the standard potential E^0 of the couple involved, and λ is the reorganization energy between the oxidized and reduced forms following electron transfer.

Since the six iron complexes used in this study do not undergo substitution readily, they probably react by an outer-sphere mechanism, in which the reorganization of the primary solvation sphere makes the chief contribution to λ. We assume in the discussion below that the λ values for all six systems are comparable to the measured value for the ferri-/ferrocyanide couple, which is 0.4 eV.[37]

A. H_2Pc Electrodes. Figure 11 shows energy level diagrams for three of the six iron complexes. The frames show data for systems ranging from the most negative to the most positive couple, and one can see that the position of $E^{0\prime}$ controls the overlap between the redox states of the electroactive species and the valence band. As $E^{0\prime}$ becomes more positive, the overlap improves; hence one can expect improved kinetics for charge transfer, just as we have observed.

Figure 11c typifies the cases with standard potentials such that both $W_{red}(U)$ and $W_{ox}(U)$ are well matched with the valence band edge of H_2Pc at the surface, U_V^s. Thus the electrode is degenerate, or virtually so, when the potential reaches the region of electrochemical activity, and one observes facile kinetics. When $W_{red}(U)$ is well matched with U_V^s, but $W_{ox}(U)$ shows poor overlap, the current-potential curve can be controlled by the valence conduction mechanism, by charge

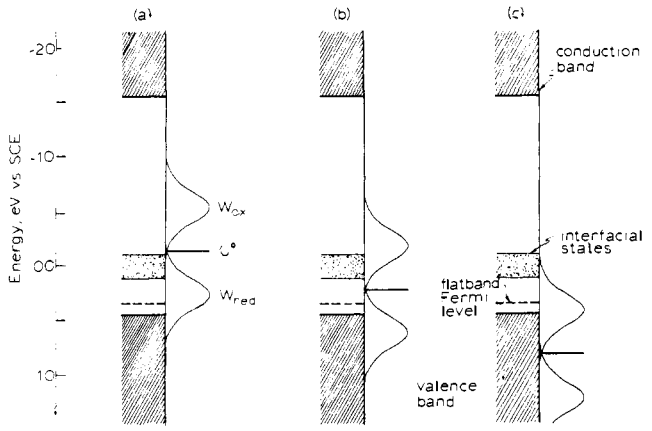

Figure 11. Energy band diagrams for electrochemical systems involving H_2Pc. Surface levels only are shown. Band bending is not depicted. (a) For $Fe(EDTA)^{-/2-}$. (b) For $Fe(CN)_6^{3-/4-}$. (c) For $Fe(o\text{-}ph)_3^{3+/2+}$.

transfer through the interfacial states, or by both, depending on the reorganization parameter.

For compounds with $E^{0\prime}$ more positive than the flatband potential, as in Figure 11a, the rate constant for oxidation via the valence band can be expressed[20,21,37]

$$k_{ox} = \kappa W_{red}(U_V^s)p_s \qquad (5)$$

where $W_{red}(U_V^s)$ is the density per unit volume of reduced species in solution having available electrons within $2kT$ of the valence band edge, p_s is the density of holes at the surface, and κ is a constant involving the cross section for hole capture. At relatively negative potentials the oxidation current is small because p_s is small. As the electrode potential becomes more positive, the rate increases due to increasing p_s until the process becomes diffusion controlled. For ferrocyanide and $Fe^{II}EDTA$, diffusion-controlled reactions are not observed until the potential is more positive than the flatband value, because the holes are depleted at the surface in the more negative potential regime.

In both of these cases, rereduction of the oxidized forms is not likely to take place via the valence band, because $W_{ox}(U)$ is poorly matched with U_V^s, as one can see from Figures 11a and 11b. For ferricyanide, $W_{ox}(U_V^s)$ is only about 10^{-5} times the maximal value of W_{ox}. An even smaller value would apply to $Fe^{III}EDTA$. One can therefore anticipate the very sluggish reductions that are actually observed.

The degree of reduction that does take place probably involves the interfacial states. The rate of reduction would then be controlled by (a) the extent of the overlap between W_{ox} and the interfacial state distribution and (b) the occupancy of the states. The overlap for ferricyanide is much better than for $Fe^{III}EDTA$, and this factor may be largely responsible for the more facile reduction of ferricyanide. Both reductions may be inhibited in part by the slow rate of movement of minority carriers from the bulk of the phthalocyanine into the space charge region (see above.) A fuller discussion of the issues involved here is available elsewhere.[38]

B. ZnPc and NiPc Electrodes. The valence band edge of ZnPc is about 0.36 V vs. SCE, and two sets of interfacial states are located near −0.20 and −0.60 V vs. SCE. With a standard potential of 0.23 V vs. SCE, ferrocyanide can be easily oxidized at ZnPc electrodes without mediating interfacial states, which show good overlap with $W_{ox}(U)$. Since the impedance measurements suggest that minority carriers can be collected into the interfacial region with relative facility (see above), rereduction of ferricyanide should occur fairly easily. Thus we could expect this system to show fairly reversible cyclic voltammograms, and it does.

The standard potential of the couple involving EDTA is −0.13 V vs. EDTA; hence there should be a significant overlap of $W_{red}(E)$ with both the intermediate levels and the valence band of ZnPc. Numerically, W_{red} at the interfacial state energy (−0.20 V vs. SCE for one set) is about 7×10^{-2} of its maximum value. The maximum itself would fall only about 0.1 V above the valence band edge. W_{ox} is poorly matched with the valence band but excellently overlaps both sets of interfacial states. Thus facile oxidation can occur once the pseudo-Fermi energy in the interior of the electrode approaches or falls below the energy of the interfacial states. More rapid hole exchange can occur when the pseudo-Fermi level reaches the valence band edge at the surface. Two anodic peaks can be observed if the oxidation due to the charge exchange via the interfacial states is not sufficiently fast to become diffusion controlled. Rereduction of $Fe\text{-}EDTA^-$ apparently cannot occur via the valence band owing to the poor overlap between W_{ox} and the valence band. However, it can occur via the interfacial states because of the excellent match between the energy levels and the relatively fast exchange of minority carriers between the interfacial region and the bulk.

A similar mechanism probably applies to the case of NiPc electrodes, since similar cyclic voltammetric behavior is observed at ZnPc and NiPc electrodes, even though there is no strong evidence for discrete bands of interfacial states in NiPc.

In support of this interpretation of the doublet oxidation waves for $Fe^{II}EDTA$, we note that the second anodic peak at ZnPc occurs at about 0.35 V vs. SCE, which corresponds to an energy of 5.10 eV vs. vacuum level. This is the energy corresponding to the valence band edge of ZnPc.[19] The second anodic peak at a NiPc electrode is around 0.30 V vs. SCE. The valence band edge of NiPc can thus be estimated to be 5.05 eV vs. vacuum.

C. Time Dependence of Voltammograms. Figure 2 illustrates the substantial dependence of voltammetric response on the waiting time between sweeps. The origin of this effect is obscure, but it probably manifests the slow charge-transfer kinetics between the interfacial states of H_2Pc and the electroactive species, as well as the slow collection of minority carriers into the interfacial region. Metal-free phthalocyanine has a flatband potential more positive than $E^{0\prime}$ for ferri-/ferrocyanide; hence a depletion layer will exist at equilibrium. Since electron filling of the interfacial states through collection from the bulk or through electron injection from ferrocyanide is slow, the time constant for reaching equilibrium may be rather long. It could be longer than 5 min for the case at hand. When the potential moves positively in the first scan, holes start to accumulate at the surface, but hole trapping in the interfacial states would compete with hole exchange between the valence band and ferrocyanide. A diffusion-limited anodic reaction could therefore occur only at a more positive potential. In the subsequent cycles, most interfacial states would stay in an unoccupied state during the time scale of the cyclic voltammetric measurement; hence fewer holes would be trapped on the positive scans. The electrode reaction should then become diffusion limited at earlier stages, until a steady state is finally reached.[39] This whole mechanism could become very complicated, if empty or occupied acceptor sites can redistribute themselves in response to potential changes, as we suggested above.

Final Remarks. The foregoing discussion shows that virtually all of our observations can be rationalized plausibly within the framework of a semiconductor model. Some aspects of the model, e.g., the possible mobility of acceptor sites and the generally low carrier mobilities, are unconventional for semiconductor electrodes. Yet, when one takes into account the very small grain sizes (which must lead to a high density of recombination centers) and the completely adventitious doping

characteristics, these materials perform remarkably straightforwardly. Our observations suggest that the electronic properties of the phthalocyanines will be important to catalytic studies involving them either as bulk solids or as films of thickness greater than ~100 Å.

Acknowledgment. We are grateful to the National Science Foundation for supporting this work via Grant CHE-78-00584.

References and Notes

(1) R. Jasinski, *Nature (London)*, **201**, 1212 (1964).
(2) See ref 3-7 for extensive recent collections of citations for this field.
(3) M. Savy, C. Bernard, and G. Magner, *Electrochim. Acta*, **20**, 383 (1975).
(4) A. J. Appleby and M. Savy in Proceedings of the Symposium on Electrode Materials and Processes for Energy Conversion and Storage, Electrochemical Society, Princeton, N.J., 1977.
(5) A. J. Appleby and M. Savy, *Electrochim. Acta*, **22**, 1315 (1977).
(6) J. Zagel, R. K. Sen, and E. Yeager, *J. Electroanal. Chem.*, **83**, 207 (1977).
(7) H. Tachikawa and L. R. Faulkner, *J. Am. Chem. Soc.*, **100**, 4379 (1978).
(8) H. Meier, W. Albrecht, V. Tschirwitz, and E. Zimmerhackl, *Ber. Bunsenges. Phys. Chem.*, **77**, 843 (1973).
(9) G. A. Alferov and V. I. Sevast'yanov, *Elektrokhimiya*, **11**, 827 (1975).
(10) S. Meshitsuka and K. Tamaru, *J. Chem. Soc., Faraday Trans. 1*, **73**, 236 (1977).
(11) F. Gutmann and L. E. Lyons, "Organic Semiconductors", Wiley, New York, 1967.
(12) S. E. Harrison and K. H. Ludewig, *J. Chem. Phys.*, **45**, 343 (1966).
(13) S. E. Harrison, *J. Chem. Phys.*, **50**, 4739 (1969).
(14) A. Sussman, *J. Appl. Phys.*, **38**, 2738 (1967).
(15) M. I. Fedorov and V. A. Benderskii, *Sov. Phys.-Semicond. (Engl. Transl.)*, **2**, 580 (1968).
(16) M. I. Federov and V. A. Benderskii, *Sov. Phys.-Semicond. (Engl. Transl.)*, **4**, 1198 (1971).
(17) M. I. Fedorov and V. A. Benderskii, *Sov. Phys.-Semicond. (Engl. Transl.)*, **4**, 1720 (1971).
(18) A. K. Ghosh, D. L. Morel, T. Feng, R. F. Shaw, and C. A. Rowe, Jr., *J. Appl. Phys.*, **45**, 230 (1974).
(19) F. R. Fan and L. R. Faulkner, *J. Chem. Phys.*, **69**, 3334, 3341 (1978).
(20) H. Gerischer, *Adv. Electrochem. Electrochem. Eng.*, **1**, 139 (1961).
(21) H. Gerischer in "Physical Chemistry: an Advanced Treatise", Vol. 9A, H. Eyring, D. Henderson, and W. Jost, Eds., Academic Press, New York, 1970.
(22) V. A. Myamlin and Yu. V. Pleskov, "Electrochemistry of Semiconductors", Plenum Press, New York, 1967.
(23) S. N. Frank and A. J. Bard, *J. Am. Chem. Soc.*, **97**, 7427 (1975).
(24) P. A. Kohl and A. J. Bard, *J. Am. Chem. Soc.*, **99**, 7532 (1977).
(25) The thicknesses reported here are based on an assumed phthalocyanine film density of unity. There is evidence that the actual densities are closer to 1.5; hence the true thicknesses may be ~30% lower than reported here. See ref 7 and 19.
(26) P. Delahay, "Double Layer and Electrode Kinetics", Wiley-Interscience, New York, 1966.
(27) P. Delahay, "New Instrumental Techniques in Electrochemistry", Wiley-Interscience, New York, 1954.
(28) T. O. Rouse and J. L. Weininger, *J. Electrochem. Soc.*, **113**, 184 (1966).
(29) D. M. Tench and E. Yeager, *J. Electrochem. Soc.*, **120**, 164 (1973).
(30) J. P. Randin, *Electrochim. Acta*, **19**, 87 (1974).
(31) W. Shockley, *Bell Syst. Tech. J.*, **28**, 435 (1949).
(32) This value is the average of values reported by R. M. Royes, *J. Am. Chem. Soc.*, **84**, 513 (1962), and by F. Lohmann, *Z. Naturforsch. A*, **22**, 843 (1967).
(33) F. I. Vilesov, A. A. Zagrubskii, and D. Z. Garbuzov, *Sov. Phys.-Solid State (Engl. Transl.)*, **5**, 1460 (1964).
(34) M. Pope, *J. Chem. Phys.*, **36**, 2810 (1962).
(35) G. S. Zhdanov and Yu. M. Vorona, *Izv. Akad. Nauk SSSR, Ser. Fiz.*, **27**, 1239 (1963).
(36) W. Katz, C. A. Evans, Jr., D. R. Eaton, and L. R. Faulkner, *J. Vac. Sci. Technol.*, **15**, 1561 (1978).
(37) R. Memming and F. Möllers, *Ber. Bunsenges. Phys. Chem.*, **76**, 475 (1972).
(38) F.-R. Fan, Ph.D. Thesis, University of Illinois at Urbana-Champaign, 1978.
(39) Note that this idea also explains the crossing effect seen in the first scan of Figure 2.

Molecular Beam Electric Deflection Behavior and Polarity of Hydrogen-Bonded Complexes of ROH, RSH, and RNH

J. A. Odutola, R. Viswanathan, and T. R. Dyke*

Contribution from the Department of Chemistry, University of Oregon, Eugene, Oregon 97403. *Received July 3, 1978*

Abstract: Molecular beam electric deflection experiments have been carried out for the dimers and higher polymers of CH_3OH, C_2H_5OH, H_2S, CH_3SH, CH_3NH_2, and $(CH_3)_2NH$. The dimers of these molecules are all found to be polar, in agreement with single, linear hydrogen bond structures. The electric deflection results for trimers and higher polymers are found to be consistent with cyclic structures.

Introduction

These studies are concerned with the conformation of hydrogen-bonded polymers of first-row hydrides and methyl and ethyl substituted hydrides. The structure of these small-molecule, hydrogen-bonded systems are of considerable theoretical[1,2] and experimental interest.[3-6] By understanding the nature of hydrogen bonding in these relatively simple molecules, it may be possible to understand in some detail the influence of hydrogen bonding in complicated systems such as macromolecules and condensed phases.

The alcohols, and to a lesser extent the amines and H_2S, have been the subject of a number of infrared vibrational spectroscopic studies in the gas phase, in inert gas and nitrogen matrices, and in various solvents. The interpretation of these results has not been entirely consistent. van Thiel et al.[5] suggested a cyclic and probably planar dimer, cyclic trimer, and open-chain higher polymers for methanol based on IR studies in a nitrogen matrix. Barnes and Hallam[4] interpreted their results for methanol in an argon matrix as consistent with an open dimer, trimer, and tetramer and a cyclic tetrameric species. Bellamy and Pace[7] proposed an open dimer (and cyclic higher polymers) from methanol solution IR spectra. Inskeep et al.[8,9] suggested that IR studies of vapor-phase methanol were best interpreted with a model consisting of open dimers and cyclic tetramers, with little or no trimer being present. Considerably less work has been done on amines and mercaptans, although we note the matrix isolation work of Tursi and Nixon,[3] who proposed an open-chain structure for $(H_2S)_2$.

Molecular beam electric deflection and electric resonance experiments[10-12] and ab initio calculations[1,13,14] on HF, H_2O, and NH_3 have shown, with impressive quantitative agreement, that the dimers of these molecules have open, linear hydro-

0002-7863/79/1501-4787$01.00/0